Amplitude Sensing below the Zero-Point Fluctuations with a Two-Dimensional Trapped-Ion Mechanical Oscillator

K. A. Gilmore,[1,2,*] J. G. Bohnet,[1] B. C. Sawyer,[3] J. W. Britton,[4] and J. J. Bollinger[1,†]
[1]National Institute of Standards and Technology, Boulder, Colorado 80305, USA
[2]JILA and Department of Physics, University of Colorado, Boulder, Colorado 80309, USA
[3]Georgia Tech Research Institute, Atlanta, Georgia 30332, USA
[4]U.S. Army Research Laboratory, Adelphi, Maryland 20783, USA
(Received 15 March 2017; revised manuscript received 21 April 2017; published 29 June 2017)

We present a technique to measure the amplitude of a center-of-mass (c.m.) motion of a two-dimensional ion crystal of ∼100 ions. By sensing motion at frequencies far from the c.m. resonance frequency, we experimentally determine the technique's measurement imprecision. We resolve amplitudes as small as 50 pm, 40 times smaller than the c.m. mode zero-point fluctuations. The technique employs a spin-dependent, optical-dipole force to couple the mechanical oscillation to the electron spins of the trapped ions, enabling a measurement of one quadrature of the c.m. motion through a readout of the spin state. We demonstrate sensitivity limits set by spin projection noise and spin decoherence due to off-resonant light scattering. When performed on resonance with the c.m. mode frequency, the technique demonstrated here can enable the detection of extremely weak forces (< 1 yN) and electric fields (< 1 nV/m), providing an opportunity to probe quantum sensing limits and search for physics beyond the standard model.

DOI: 10.1103/PhysRevLett.118.263602

Measuring the amplitude of mechanical oscillators has engaged physicists for more than 50 years [1,2] and, as the limits of amplitude sensing have dramatically improved, has produced exciting advances both in fundamental physics and in applied work. Examples include the detection of gravitational waves [3], the coherent quantum control of mesoscopic objects [4], improved force microscopy [5], and the transduction of quantum signals [6]. During the past decade, optomechanical systems have facilitated increasingly sensitive techniques for reading out the amplitude of a mechanical oscillator [7–11], with a recent demonstration obtaining a measurement imprecision more than 2 orders of magnitude below z_{ZPT}, the amplitude of the ground-state zero-point fluctuations [12]. Optomechanical systems have assumed a wide range of physical systems, including toroidal resonators, nanobeams, and membranes, but the basic principle involves coupling the amplitude of a mechanical oscillator to the resonant frequency of an optical cavity mode [4].

Crystals of laser-cooled, trapped ions behave as atomic-scale mechanical oscillators [13–15] with tunable oscillator modes and high quality factors ($\sim 10^6$). Furthermore, laser cooling enables ground-state cooling and nonthermal state generation of these oscillators. Trapped-ion crystals therefore provide an ideal experimental platform for investigating the fundamental limits of amplitude sensing. Prior work has demonstrated the detection of coherently driven amplitudes larger than the zero-point fluctuations of the trapped-ion oscillator [14–16], and has reported impressive force sensing by injection locking an optically amplified oscillation of a single trapped ion [17].

In this Letter we experimentally and theoretically analyze a technique to measure the center-of-mass (c.m.) motion of a two-dimensional, trapped-ion crystal of ∼100 ions with a sensitivity below z_{ZPT}. We employ a time-varying spin-dependent force $F_0 \cos(\mu t)$ that couples the amplitude of the c.m. motion with the internal spin degree of freedom of the ions [18–20]. When the frequency μ matches the frequency ω of a driven c.m. oscillation, $Z_c \cos(\omega t)$, a spin precession proportional to Z_c occurs. The amplitude-dependent spin precession is analogous to the optomechanical frequency shift of a cavity mode. In contrast to the continuous measurement typical of optomechanics experiments, we measure the spin precession only at the end of the experimental sequence, with a precision imposed by spin projection noise [21].

To determine the readout imprecision in a regime free from thermal noise, we perform measurements where ω is far from resonance with the trap axial frequency ω_z. Additionally, we implement a protocol where the phase of the measured quadrature randomly varies from one iteration of the experiment to the next, appropriate for sensing a force whose phase is unknown or not stable. For $N = 85$ ions and $z_{\mathrm{ZPT}} \equiv (1/\sqrt{N})\sqrt{(\hbar/2m\omega_z)} \approx 2$ nm, we detect amplitudes $Z_c = 500$ pm in a single implementation of the experimental sequence, and as small as 50 pm after averaging over 3000 iterations of the sequence.

Our experimental apparatus, described in Fig. 1 and Refs. [18,19,22], consists of $N \sim 100$ $^9\mathrm{Be}^+$ ions laser cooled to the Doppler limit of 0.5 mK and confined to a single-plane Coulomb crystal in a Penning trap. The spin-1/2 degree of freedom is the $^2S_{1/2}$ ground-state valence

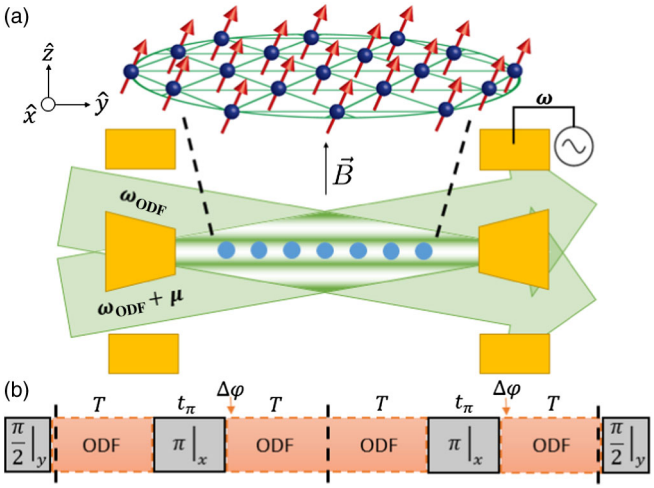

FIG. 1. (a) Representation of ion spins arranged in a 2D triangular lattice, along with a cross-section illustration of the Penning trap, characterized by an axial magnetic field $B = 4.45$ T and an axial trap frequency $\omega_z = 2\pi \times 1.57$ MHz. The blue dots represent ions. Cylindrical electrodes (yellow) generate a harmonic confining potential along the $\hat{z}$ axis. Radial confinement is provided by the Lorentz force from $(\vec{E} \times \vec{B})$-induced rotation in the axial magnetic field. The beams generating the spin-dependent optical-dipole force (the green arrows) cross the ion plane at $\pm 10°$, forming a 1D traveling-wave potential (the green lines) with $\delta k = 2\pi/(0.9\ \mu\text{m})$. An ac voltage source is connected to the trap end cap and used to drive an axial oscillation with calibrated amplitude Z_c. (b) Quantum lock-in CPMG sequence used to detect spin precession produced by c.m. motion resonant with the ODF. Doppler cooling and $|\uparrow\rangle_N$ spin-state preparation occur before the sequence, and spin-state detection after. The grey blocks with solid borders represent microwave $\pi/2$ rotations around $\hat{y}$ and π rotations around $\hat{x}$. The orange blocks with dashed borders represent ODF pulses. The ODF phase is advanced by $\Delta\varphi$ in a modulation scheme discussed in Ref. [23], where $\Delta\varphi = \pi$ for $\omega = \mu$. The dashed vertical lines indicate the m segments of the sequence (here, $m = 2$). We make use of an $m = 8$ sequence for Figs. 2–4.

electron spin $|\uparrow\rangle(|\downarrow\rangle) \equiv |m_s = +1/2\rangle(|m_s = -1/2\rangle)$. In the magnetic field of the Penning trap, the spin-flip frequency is 124 GHz. A resonant microwave source is used to perform global rotations of the spin ensemble. A pair of laser beams, detuned from the nearest optical transitions by ~20 GHz, interfere to form a one-dimensional (1D) traveling-wave potential that produces a spin-dependent optical-dipole force (ODF). Optical pumping prepares the initial state $|\uparrow\rangle_N \equiv |\uparrow\uparrow\cdots\uparrow\rangle$ with high fidelity. At the end of the experiment, we measure the probability $P_\uparrow$ for an ion spin to be in $|\uparrow\rangle$ from a global measurement of state-dependent resonance fluorescence on the Doppler cooling transition, where spin $|\uparrow\rangle$ ($|\downarrow\rangle$) is bright (dark).

If the ions are localized axially over an extent that is small compared to the wavelength of the 1D traveling-wave potential (Lamb-Dicke confinement), then the ODF couples the spin and motional degrees of freedom through the interaction [22]

$$\hat{H}_{\text{ODF}} = F_0 \cos(\mu t) \sum_i \hat{z}_i \hat{\sigma}_i^z. \tag{1}$$

Here, $F_0 = U\,\delta k\,\text{DWF}$ is the magnitude of the ODF, where $U(\delta k)$ is the zero-to-peak potential (wave vector) of the 1D traveling wave, μ is the frequency difference between the ODF beams, and $\hat{z}_i$ and $\hat{\sigma}_i^z$ are the position operator and the Pauli spin matrix for ion i. The Debye-Waller factor $\text{DWF} = \exp(-\delta k^2 \langle \hat{z}_i^2 \rangle/2)$ reduces F_0 due to the departure from the Lamb-Dicke confinement regime [24]; $\text{DWF} \approx 0.86$ for the conditions of this work. The potential U, and therefore F_0, is determined from ac Stark shift measurements on the ions [25]. Typical maximum values for this work are $U/\hbar \approx 2\pi \times (10.4\,\text{kHz})$, resulting in $F_0 \approx 40$ yN.

Equation (1) describes a dependence of the spin transition frequency on the axial position of the ions and the ODF frequency μ. We excite a small, classically driven c.m. motion of constant amplitude $\hat{z}_i \to \hat{z}_i + Z_c \cos(\omega t + \delta)$ with a weak rf drive on a trap end-cap electrode [see Fig. 1(a)] at a frequency ω far from ω_z. If $\omega \sim \mu$, Eq. (1) produces an approximately constant shift in the spin transition frequency. With $\delta k Z_c \ll 1$, this shift is given by

$$\hat{H}_{\text{ODF}} \approx F_0 Z_c \cos[(\omega - \mu)t + \delta] \sum_i \frac{\hat{\sigma}_i^z}{2}. \tag{2}$$

For $\mu = \omega$, the static shift of the spin transition frequency is simply $\Delta(Z_c) = (F_0/\hbar) Z_c \cos(\delta)$.

We measure $\Delta(Z_c)$ from the resulting spin precession in an experiment like that shown in Fig. 1(b). Ideally, spin precession can be measured using a Ramsey-type experiment. First, the ions are prepared in the $|\uparrow\rangle_N$ state, followed by a microwave $\pi/2$ pulse around $\hat{y}$ that rotates the spins to the $\hat{x}$ axis. The spins precess for an interaction time τ so that the resulting spin precession on resonance ($\mu = \omega$) is $\theta = \theta_{\text{max}} \cos(\delta)$, where $\theta_{\text{max}} \equiv (F_0/\hbar) Z_c \tau$. After a final $\pi/2$ pulse around $\hat{y}$, the final state readout measures the population of the spins in $|\uparrow\rangle$, $P_\uparrow = \frac{1}{2}[1 - e^{-\Gamma\tau} \cos(\theta)]$. Here, Γ is the decay rate from spontaneous emission from the off-resonant ODF laser beams [26]. To detect small amplitudes with the available F_0 in our setup, we extend the spin-precession time to $\tau \geq 20$ ms. To avoid decoherence due to magnetic field fluctuations and coherently accumulate spin precession, we use a quantum lock-in [27] sequence where, during the interaction time τ, the spin precession is interrupted by a train of π pulses that are synchronized with phase jumps enforced on the ODF beams [23]. Specifically, we use a Carr-Purcell-Meiboom-Gill (CPMG) sequence with $m = 8$ ODF-π-ODF segments [$\tau = 2mT$, see Fig. 1(b)].

We ensure the phase δ randomly varies from one iteration of the CPMG sequence to the next, effectively measuring a random quadrature of the motion for each experimental trial. Different experimental trials therefore

result in a different precession θ, as indicated in Fig. 3. We measure the collective dephasing (or decoherence) averaged over many experimental trials $\langle P_\uparrow \rangle = \frac{1}{2}[1 - e^{-\Gamma\tau}\langle\cos(\theta)\rangle]$. Here, the brackets $\langle\cdots\rangle$ denote an average over many iterations of the CPMG sequence. Averaging over the random phase δ yields [28]

$$\langle P_\uparrow \rangle = \frac{1}{2}[1 - e^{-\Gamma\tau} J_0(\theta_{\max})], \tag{3}$$

with J_0 being the zeroth-order Bessel function of the first kind.

To create the steady-state c.m. axial oscillation $Z_c \cos(\omega t + \delta)$, we applied a continuous ac voltage to an end cap of the Penning trap at a frequency $\omega/(2\pi)$ near 400 kHz. This frequency was chosen because it was far from any motional mode frequencies of the ion crystal, and there were no observed noise sources. Thus, the background, i.e., the signal without the driven c.m. axial motion, such that $Z_c = 0$, was fully characterized by decoherence due to spontaneous emission and is given by $\langle P_\uparrow \rangle_{\text{bck}} = \frac{1}{2}[1 - e^{-\Gamma\tau}]$. We calibrated the displacement of the ions due to a static voltage applied to the end cap by measuring the resulting movement of the ion crystal in the side-view imaging system. From this calibration, we determined that a 1 V offset results in a 0.97(5) μm displacement of the ions. We estimate that the corrections for using this dc calibration to estimate Z_c for an $\omega/(2\pi) \approx 400$ kHz drive is less than 10%.

Figure 2 shows the emergence of the measured spin-precession signal out of the background as the amplitude Z_c is increased from 500 pm to 5 nm. The measured line shape agrees well with the prediction, detailed in Ref. [23], involving no free parameters. Figure 3 shows the background and the measured resonant ($\mu = \omega$) response to a $Z_c = 485$ pm oscillation for a range of ODF strengths F_0/F_{0M}, where F_{0M} is the maximum F_0 possible with our current setup (~40 yN). Agreement with Eq. (3) involving no free parameters is excellent. For both Fig. 2 and Fig. 3, the background is within 6% of that determined by independent measurements of the spontaneous emission decay rates of each ODF beam [25]. The amplitude $Z_c = \theta_{\max}/(\tau F_0/\hbar)$ can be determined from the difference $\langle P_\uparrow \rangle - \langle P_\uparrow \rangle_{\text{bck}}$ [23]. We note that $\langle P_\uparrow \rangle - \langle P_\uparrow \rangle_{\text{bck}}$ depends on $\theta^2_{\max}$. Therefore, the sensing protocol described here directly measures Z_c^2. The inset of Fig. 3 shows a determination of Z_c^2 for a range of ODF strengths. The uncertainties were calculated from the measured noise of the $\langle P_\uparrow \rangle - \langle P_\uparrow \rangle_{\text{bck}}$ measurements using standard error propagation. These uncertainties go through a minimum, indicating an optimum F_0/F_{0M} value for determining Z_c^2.

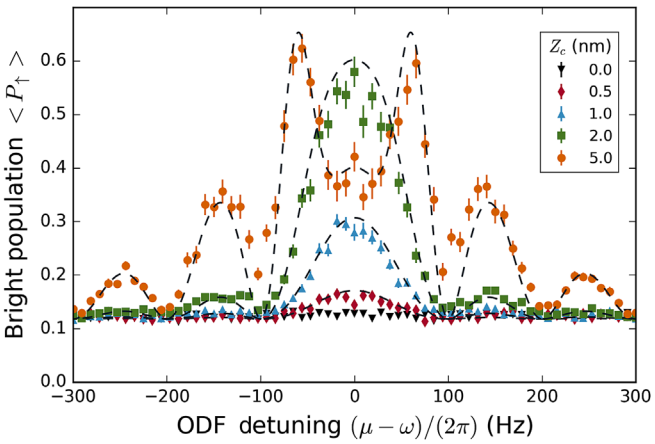

FIG. 2. Line shape of the spin-precession signal for amplitudes Z_c of 500 pm (the red diamonds), 1 nm (the blue triangles), 2 nm (the green squares), and 5 nm (the orange circles) for $\tau = 20$ ms. The black triangles are the background, with the drive turned off. The dashed lines are predictions with no free parameters. The error bars represent standard error. Here $N = 90$ ions and $F_0 = 7.9$ yN.

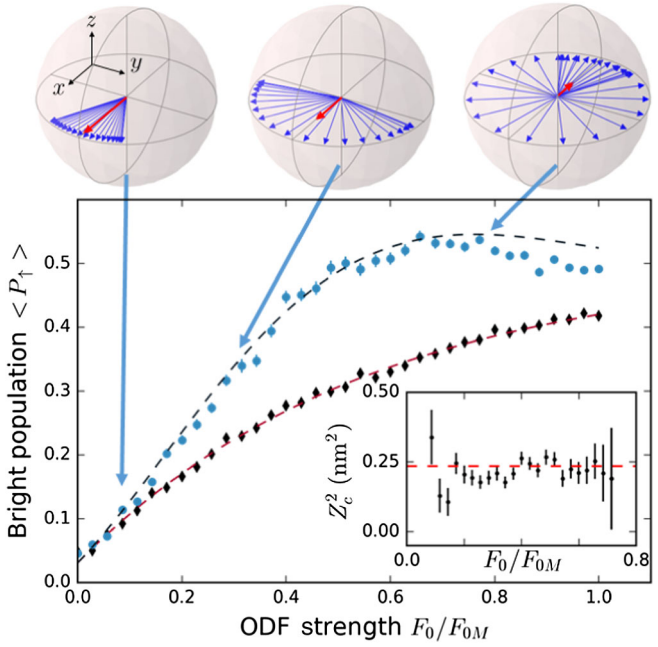

FIG. 3. (Top panels) Bloch sphere representation [29] of spin dephasing for $Z_c = 485$ pm. Each blue vector represents an experimental trial with a different phase δ (see the text). From left to right, the spread in the blue vectors corresponds to $\theta_{\max} = 0.470$, 1.41, 3.62 rad and $F_0/F_{0M} = 0.1$, 0.3, 0.77, where F_{0M} is the maximum optical-dipole force. Our experiment measures the length of the Bloch vector averaged over many trials, denoted by the thick red vector. (Main plot) As a function of ODF strength, the background (the black diamonds) with no applied drive and signal (the blue points) for a 485 pm amplitude and total ODF interaction time $\tau = 24$ ms is shown. The red dashed line is a fit to the background. The black dashed line is the prediction with no free parameters, given the background fit. Here, $N = 75$ ions and $F_{0M} = 41.3$ yN. (Inset) The black points are experimentally determined values for Z_c^2. The red dashed line is the calibrated value of Z_c^2. The error bars represent standard error.

To explore the ultimate amplitude sensing limits of our protocol, we performed repeated pairs of $P_\uparrow$ measurements, first with $Z_c = 0$ to get the background, then with $Z_c \neq 0$. For a given Z_c, 3000 pairs of measurements were used to determine the average difference $\langle P_\uparrow \rangle - \langle P_\uparrow \rangle_{\mathrm{bck}}$ and the standard deviation $\sigma(P_\uparrow - P_{\uparrow,\mathrm{bck}})$ of the difference for a single pair of measurements. For each Z_c, F_0/F_{0M} was set close to the value that maximizes the signal-to-noise ratio for determining Z_c^2. This occurs for a relatively small $\theta_{\max}$ such that $\frac{1}{2}[1 - J_0(\theta_{\max})] \approx \theta_{\max}^2/8$. Then, the signal-to-noise ratio for determining Z_c^2 from a single pair of $P_\uparrow$, $P_{\uparrow,\mathrm{bck}}$ measurements is approximately

$$\frac{Z_c^2}{\delta Z_c^2} \approx \frac{\langle P_\uparrow \rangle - \langle P_\uparrow \rangle_{\mathrm{bck}}}{\sigma(P_\uparrow - P_{\uparrow,\mathrm{bck}})}. \tag{4}$$

Figure 4 displays Eq. (4) from measurements acquired with Z_c ranging from 10 nm to as small as 0.025 nm. Excellent agreement is observed with a model (the dashed red line) that assumes the only noise sources are projection noise in the spin-state detection and fluctuations in $P_\uparrow$ produced by random variation in the phase δ from one experimental trial to the next.

For amplitudes $Z_c \gtrsim 500$ pm, fluctuations in $P_\uparrow$ due to the random variation of the phase δ for different experimental trials dominate. This situation is depicted by the middle Bloch sphere of Fig. 3. Here, the fluctuations in $P_\uparrow$ are comparable to the difference $\langle P_\uparrow \rangle - \langle P_\uparrow \rangle_{\mathrm{bck}}$, limiting the signal-to-noise ratio of a single determination of Z_c^2 to ~ 1. As Z_c decreases, this noise and the signal decrease while projection noise stays approximately the same, resulting in a decreasing $Z_c^2/\delta Z_c^2$. For a small Z_c, we show

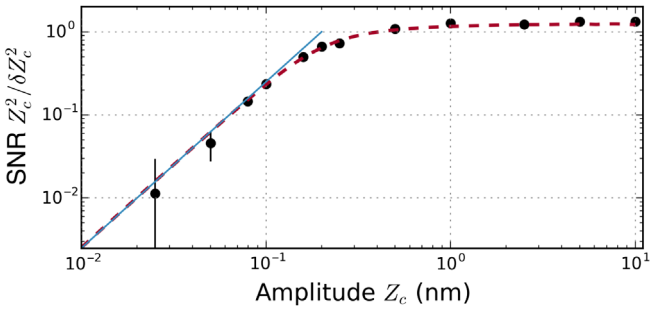

FIG. 4. Amplitude sensing limits for $N = 85$. The black points are the experimentally measured signal-to-noise ratio for determinations of Z_c^2 from single pairs of $P_\uparrow$, $P_{\uparrow,\mathrm{bck}}$ measurements as a function of the experimentally imposed Z_c. Our measurement for $Z_c = 25$ pm is consistent with zero. The red dashed line is the prediction for the signal-to-noise ratio, including projection noise and the random c.m. mode quadrature measured each trial. The blue solid line is the predicted limiting signal-to-noise ratio for small amplitudes [Eq. (5)], assuming only projection noise and parameters relevant for our setup. The error bars represent standard error.

that the sensitivity is determined by N, δk, and the ratio of the spontaneous decay rate to the optical potential $\xi \equiv \Gamma/(U/\hbar)$ [23], according to

$$\left.\frac{Z_c^2}{\delta Z_c^2}\right|_{\mathrm{limiting}} \approx 0.097 \frac{\sqrt{N}(\mathrm{DWF})^2(\delta k)^2}{\xi^2} Z_c^2. \tag{5}$$

For $N = 85$ and values of DWF, δk, and $\xi = 1.156 \times 10^{-3}$ relevant to our setup, Eq. (5) predicts $Z_c^2/\delta Z_c^2 \approx [Z_c/0.2\ \mathrm{nm}]^2$, displayed as the blue line in Fig. 4. On the log-log plot, the slope of 2 is the result of a signal proportional to Z_c^2 along with a constant readout noise of the spins (here, projection noise). We perform 16 pairs of measurements in 1 s, so the signal-to-noise ratio $Z_c^2/\delta Z_c^2 \approx [Z_c/0.2\ \mathrm{nm}]^2$ for a single pair of measurements corresponds to a long averaging time sensitivity of $(100\ \mathrm{pm})^2/\sqrt{\mathrm{Hz}}$ (recall that our protocol measures Z_c^2).

Figure 4 documents a good understanding of the sensing limits of our protocol, indicating how the measurement can be improved in the future. Equation (5) scales as $1/\xi^2$, resulting in significant improvements for setups with less spontaneous decay. By stabilizing the ODF beat-note phase with respect to the classical drive [30,31], we could repeatedly measure the same quadrature of motion and realize a substantial improvement in sensitivity. For this phase-coherent protocol, assuming that $N = 100$ and current parameters of our setup, we estimate [23] a measurement imprecision of 74 pm for a single implementation of the experimental sequence. This is ~ 30 times smaller than z_{ZPT}, producing a long averaging time sensitivity of $\sim 18\ \mathrm{pm}/\sqrt{\mathrm{Hz}}$. The use of spin-squeezed states, recently demonstrated in this system [22], can provide an additional enhancement by reducing the projection noise of the readout.

The 50 pm amplitude detected in Fig. 4 at a frequency ω far from resonance corresponds to an electric field detection of 0.46 mV/m or 73 yN/ion. These force and electric field sensitivities can be improved by the Q of the c.m. mode by probing near resonance with ω_z. Quality factors $Q \sim 10^6$ should be possible with trapped-ion c.m. modes. The detection of a 20 pm amplitude resulting from a 100 ms coherent drive on the 1.57 MHz c.m. mode is sensitive to a force per ion of 5×10^{-5} yN, corresponding to an electric field of 0.35 nV/m. Electric field sensing below ~ 1 nV/m enables searches for hidden-photon dark matter [32,33], although shielding effects must be carefully considered. Ion traps typically operate with frequencies $\omega_z/2\pi$ between 50 kHz and 5 MHz, providing a sensitivity to hidden-photon masses from 2×10^{-10} to 2×10^{-8} eV.

By sensing c.m. motion far from resonance, we calibrate the measurement imprecision of our protocol in the absence of thermal noise and backaction. Probing on resonance with a measurement imprecision below z_{ZPT} will be sensitive to thermal fluctuations and backaction due to spin-motion

entanglement [19]. This motivates the investigation of potential backaction-evading protocols with trapped-ion setups. For the phase-coherent measurement of a single quadrature, backaction due to spin-motion entanglement can be evaded through the introduction of the appropriate correlations between spin and motion [34].

In summary, we have presented a technique for amplitude sensing below z_{ZPT} of a trapped-ion mechanical oscillator. By employing a spin-dependent force to couple the spin and motional degrees of freedom of the ions, the amplitude of the c.m. motion may be determined. We have detected a 500 pm amplitude in a single experimental trial and demonstrated a long measurement time sensitivity of $(100\ \mathrm{pm})^2/\sqrt{\mathrm{Hz}}$ with a protocol where the phase of the measured quadrature randomly varies. Modifications of our setup should enable repeated measurements of the same quadrature, with a measurement imprecision of 74 pm for a single experimental trial with $N = 100$ ions, providing opportunities for trapped-ion mechanical oscillators to explore the quantum limits of amplitude and force sensing, and to enable the use of new tools in the search for physics beyond the standard model.

We thank V. Sudhir, R. Ozeri, S. Kotler, J. Teufel, J. Jaeckel, J. E. Jordan, and D. Kienzler for the stimulating discussions. K. A. G. is supported by NSF Grant No. PHY 1521080. Contributions to this Letter by workers at NIST, an agency of the U.S. Government, are not subject to U.S. copyright.

*kevin.gilmore@colorado.edu
†john.bollinger@nist.gov

[1] J. Weber, Phys. Rev. Lett. **17**, 1228 (1966).
[2] C. M. Caves, Phys. Rev. Lett. **45**, 75 (1980).
[3] B. P. Abbott *et al.* (LIGO Scientific and Virgo Collaborations), Phys. Rev. Lett. **116**, 061102 (2016).
[4] M. Aspelmeyer, T. J. Kippenberg, and F. Marquardt, Rev. Mod. Phys. **86**, 1391 (2014).
[5] H.-J. Butt, B. Cappella, and M. Kappl, Surf. Sci. Rep. **59**, 1 (2005).
[6] T. A. Palomaki, J. W. Harlow, J. D. Teufel, R. W. Simmonds, and K. W. Lehnert, Nature (London) **495**, 210 (2013).
[7] J. D. Teufel, T. Donner, M. A. Castellanos-Beltran, J. W. Harlow, and K. W. Lehnert, Nat. Nanotechnol. **4**, 820 (2009).
[8] G. Anetsberger, O. Arcizet, Q. P. Unterreithmeier, R. Rivière, A. Schliesser, E. M. Weig, J. P. Kotthaus, and T. J. Kippenberg, Nat. Phys. **5**, 909 (2009).
[9] T. Westphal, D. Friedrich, H. Kaufer, K. Yamamoto, S. Goßler, H. Müller-Ebhardt, S. L. Danilishin, F. Y. Khalili, K. Danzmann, and R. Schnabel, Phys. Rev. A **85**, 063806 (2012).
[10] S. Schreppler, N. Spethmann, N. Brahms, T. Botter, M. Barrios, and D. M. Stamper-Kurn, Science **344**, 1486 (2014).
[11] N. S. Kampel, R. W. Peterson, R. Fischer, P.-L. Yu, K. Cicak, R. W. Simmonds, K. W. Lehnert, and C. A. Regal, Phys. Rev. X **7**, 021008 (2017).
[12] D. J. Wilson, V. Sudhir, N. Piro, R. Schilling, A. Ghadimi, and T. J. Kippenberg, Nature (London) **524**, 325 (2014).
[13] J. D. Jost, J. P. Home, J. M. Amini, D. Hanneke, R. Ozeri, C. Langer, J. J. Bollinger, D. Leibfried, and D. J. Wineland, Nature (London) **459**, 683 (2009).
[14] M. J. Biercuk, H. Uys, J. W. Britton, A. P. VanDevender, and J. J. Bollinger, Nat. Nanotechnol. **5**, 646 (2010).
[15] B. C. Sawyer, J. W. Britton, A. C. Keith, C.-C. Joseph Wang, J. K. Freericks, H. Uys, M. J. Biercuk, and J. J. Bollinger, Phys. Rev. Lett. **108**, 213003 (2012).
[16] R. Shaniv and R. Ozeri, Nat. Commun. **8**, 14157 (2017).
[17] S. Knünz, M. Herrmann, V. Batteiger, G. Saathoff, T. W. Hänsch, K. Vahala, and T. Udem, Phys. Rev. Lett. **105**, 013004 (2010).
[18] J. J. Bollinger, J. W. Britton, and B. C. Sawyer, AIP Conf. Proc. **1521**, 200 (2013).
[19] B. C. Sawyer, J. W. Britton, and J. J. Bollinger, Phys. Rev. A **89**, 033408 (2014).
[20] P. A. Ivanov, Phys. Rev. A **94**, 022330 (2016).
[21] W. M. Itano, J. C. Bergquist, J. J. Bollinger, J. M. Gilligan, D. J. Heinzen, F. L. Moore, M. G. Raizen, and D. J. Wineland, Phys. Rev. A **47**, 3554 (1993).
[22] J. G. Bohnet, B. C. Sawyer, J. W. Britton, M. L. Wall, A. M. Rey, M. Foss-Feig, and J. J. Bollinger, Science **352**, 1297 (2016).
[23] See Supplemental Material at http://link.aps.org/supplemental/10.1103/PhysRevLett.118.263602 for technical details and derivations.
[24] D. J. Wineland, C. Monroe, W. M. Itano, D. Leibfried, B. E. King, and D. M. Meekhof, J. Res. Natl. Inst. Stand. Technol. **103**, 259 (1998).
[25] J. W. Britton, B. C. Sawyer, A. C. Keith, C.-C. J. Wang, J. K. Freericks, H. Uys, M. J. Biercuk, and J. J. Bollinger, Nature (London) **484**, 489 (2012).
[26] H. Uys, M. J. Biercuk, A. P. VanDevender, C. Ospelkaus, D. Meiser, R. Ozeri, and J. J. Bollinger, Phys. Rev. Lett. **105**, 200401 (2010).
[27] S. Kotler, N. Akerman, Y. Glickman, A. Keselman, and R. Ozeri, Nature (London) **473**, 61 (2011).
[28] S. Kotler, N. Akerman, Y. Glickman, and R. Ozeri, Phys. Rev. Lett. **110**, 110503 (2013).
[29] J. R. Johansson, P. D. Nation, and F. Nori, Comput. Phys. Commun. **183**, 1760 (2012).
[30] D. B. Hume, C. W. Chou, D. R. Leibrandt, M. J. Thorpe, D. J. Wineland, and T. Rosenband, Phys. Rev. Lett. **107**, 243902 (2011).
[31] M. J. Biercuk, H. Uys, J. W. Britton, A. P. VanDevender, and J. J. Bollinger, Opt. Express **19**, 10304 (2011).
[32] P. Arias, D. Cadamuro, M. Goodsell, J. Jaeckel, J. Redondo, and A. Ringwald, J. Cosmol. Astropart. Phys. 06 (2012) 013.
[33] S. Chaudhuri, P. W. Graham, K. Irwin, J. Mardon, S. Rajendran, and Y. Zhao, Phys. Rev. D **92**, 075012 (2015).
[34] C. Hempel, B. P. Lanyon, P. Jurcevic, R. Gerritsma, R. Blatt, and C. F. Roos, Nat. Photonics **7**, 630 (2013).